AIAA 7th Aerospace Sciences Meeting, AIAA Paper 69-96, New York, Jan. 1969.

[4]McLain, A. G., and Rao, C. S. R., "A Hybrid Computer Program for Rapidly Solving Flowing or Static Chemical Kinetics Involving Many Chemical Species," NASA TM X-3403, July 1976.

Numerical Study of Unsteady Supersonic Compression Ramp Flows

S. O. Park,* Y. M. Chung,† and H. J. Sung‡
Korea Advanced Institute of Science and Technology, Taejon 305-701, Republic of Korea

Introduction

TWO-DIMENSIONAL, steady, inviscid, supersonic flows past a compression ramp are very well known. However, unsteady flows past a moving compression ramp with time varying wedge angle have received scant attention and are thus little understood. Degani and Steger[1] touched upon the compression-ramp flow where the ramp moved from 15 to 20 deg at a constant angular velocity. In that work, the main interest was the comparison between the thin-layer and the Navier-Stokes computation. We intend in this work to investigate inviscid supersonic flow past a moving compression ramp by numerically solving the Euler equations. The flow configuration is schematically shown in Fig. 1a. Despite its simple geometry, such a flow can hardly be tackled by analytical means since linearization is not allowed. The wedge angle varies linearly with time from 0 deg up to a given angle. When the wedge angle reaches the final value, the ramp motion ceases. The flow configuration may be considered as a fundamental problem for transient flow of a thrust vectoring nozzle or a maneuvering high-speed wing. Important parameters for the present flow are the free stream Mach number M_∞, the angular velocity of the wedge Ω, and the final wedge angle Θ_f. A pertinent dimensionless parameter from these variables is the reduced angular velocity $\bar{\Omega}$ defined by the relation $\bar{\Omega} = \Omega L/M_\infty a_\infty$, where L is a reference length. The flow is anticipated to change significantly with $\bar{\Omega}$ and thus several typical values of were considered in this work.

Numerics

The equations to be solved are the two-dimensional Euler equations in conservation form. When the governing equation is integrated over a fixed control volume A with boundary surface C, we obtain

$$\iint_A \left(\frac{\partial w}{\partial t}\right) dA + \oint_C (f\,dy - f\,dx) \tag{1}$$

where $w = (\rho, \rho u, \rho v, \rho e)^T$, and f and g are appropriate flux vectors corresponding to w (Ref. 2).

When the control volume is moving with velocity, where $\zeta = (\xi, \eta)^T$, the material derivative of volume integral can be written as follows via the Reynolds' transport theorem:

$$\frac{d}{dt}\iint_{A(t)} w\,dA = \iint_A \left(\frac{\partial w}{\partial t}\right) dA + \int_C w(\zeta \cdot \boldsymbol{n})\,ds \tag{2}$$

Received Dec. 31, 1992; presented as Paper 93-0883 at the AIAA 31st Aerospace Sciences Meeting, Reno, NV, Jan. 11–14, 1993; revision received June 8, 1993; accepted for publication June 12, 1993.

*Professor, Department of Aerospace Engineering, 373-1 Kusong-Dong, Yusung-Ku. Member AIAA.

†Research Assistant, Department of Mechanical Engineering, 373-1 Kusong-Dong, Yusung-Ku.

‡Associate Professor, Department of Mechanical Engineering, 373-1 Kusong-Dong, Yusung-Ku.

Using Eq. (2), Eq . (1) can be written for a moving control volume as[3]

$$\frac{d}{dt}(Aw) + qw = 0 \tag{3}$$

where A is the area of a grid cell and

$$qw = \oint_C [(f - w\xi)\,dy - (g - w\eta)\,dx] + \text{artificial dissipation terms} \tag{4}$$

For the artificial dissipation terms, we adopted Jameson's second- and fourth-order expressions[4,5] Equation (3) was integrated using the fourth-order Runge-Kutta time-stepping scheme.[4] For inflow and upper far boundaries, free-stream conditions were specified. Outflow boundary values were specified using second-order extrapolation from the interior node values. Transient solutions were obtained by time-marching Eq. (3) with uniform flow at time $t = 0$. The grid system over the surface of the wedge moves in the x and y directions with the speed of the moving wedge. Preliminary computations were carried out for the case of $\bar{\Omega} = 0.1$ for the wedge with $M_\infty = 2$ and $\Theta_f = 20$ deg on 40×40, 60×60, and 80×80 mesh systems. All of the three mesh systems performed to yield solutions accurate within 0.5% compared with the analytic solutions for the steady flow. However, for the unsteady flow, the solutions with the 40×40 mesh system were of poor quality when compared with the solutions with the 60×60 and 80×80 mesh systems. The solutions with the 80×80 mesh system were essentially the same as those with the 60×60 mesh system. Thus, we chose the 60×60 mesh system for the present work. The time increment Δt (for the unsteady calculations) was chosen to make the Courant-Friedrichs-Lewy (CFL) number be 0.1 when $\bar{\Omega} = 1.0$ and 0.2 when $\bar{\Omega} = 0.1$ or smaller. The solutions of the exploratory computations with the CFL number of 0.5 exhibited spurious wiggles across the shock wave during the motion of the ramp. Since the present computation required time accurate solutions, we conservatively chose CFL numbers to be small as stated earlier.

Results and Discussion

The transient solutions were obtained for the cases of four different values of angular velocity $\bar{\Omega}$ with $M_\infty = 2$, and $\Theta_f = 20$ deg.

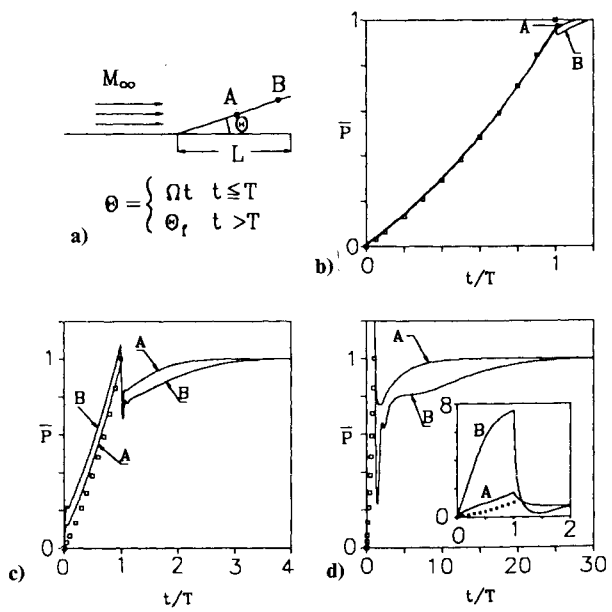

Fig. 1 Flow configuration and surface pressure variation $\{\bar{p} = (p - p_\infty)/[p(t = \infty)] - p_\infty\}$: a) schematic, b) $\bar{\Omega} = 0.01$, c) $\bar{\Omega} = 0.1$, and d) $\bar{\Omega} = 1.0$.

The four values of the reduced angular velocity $\bar{\Omega}$ were 0.001, 0.01, 0.1, and 1.

Figures 1b-1d compare the pressure variation with time at two points (see Fig. 1a) of the surface of the ramp. The data marked by the open symbol are the pressure obtained by the steady oblique shock relation for the wedge having the same angle as the instantaneous angle of the moving ramp. When the ramp moves very slowly, the flow can be regarded as steady or quasi-steady. Thus, when $\bar{\Omega}$ was 0.001, the pressure changed in the same manner as if the ramp had been stationary. When $\bar{\Omega}$ was 0.01, the transient flow establishment was only slightly different from that of the case of $\bar{\Omega}$ = 0.001. We see in Fig. 1b that the pressure change with wedge angle are about the same as that for the steady case.

Figure 1c and 2 illustrate, respectively, the surface pressure variation and the sequential flow development for the case of $\bar{\Omega}$ = 0.1. The dashed lines in Fig. 2 represent the shock wave angle obtained through the oblique shock relation for the corresponding steady ramp. At the initial stage of flow development, the compression waves are curved rather than straight. An oblique shock first appears near the compression corner (Fig. 2b). Away from the corner, pressure gradient across the isobars is rather mild. After the ramp motion ceases, the flow relaxes to the final steady state over a considerable time period. The oblique shock wave during the relaxation process is curved and the wave angle is smaller than the final wave angle as can be seen in Fig. 2d. At about $t = 4T$, the flow became essentially steady. The surface pressure curves of Fig. 1c indicate that the pressure of the moving ramp is a little higher than that of the corresponding steady flow. We note that the pressure at point B is higher than that at point A, which reflects the faster linear speed of the upward motion of the ramp at B. Immediately after the ramp motion ceases, the surface pressure drops rapidly owing to the impulsive stop of the ramp. After the sudden drop, the pressure gradually rises to its steady state value. It is noted that the pressure at B just after the stop of the ramp is smaller than the pressure at A, which signifies that the "impulsiveness" of the ramp stop felt by the flow at B is much stronger than at A. When $\bar{\Omega}$ = 1.0, the departure of the unsteady flow from the corresponding steady flow becomes very drastic. The surface pressure variation (Fig. 1d and insert : the insert depicts the detailed pressure variation during the ramp motion that is not clearly seen in the main figure) and the isopressure contours (Fig. 3) illustrate this situation. In Fig. 1d, we see that the surface pressure is much higher than the corresponding steady state value. However, the nature of the pressure overshoot and the relaxation process after the stop of the ramp are qualitatively similar to those for the case of $\bar{\Omega}$ = 0.1. The isopressure contours of Fig. 3a show that a steep pressure gradient layer, which may be viewed as a shock wave, is confined in the narrow region close to the moving wall. Figure 3b illustrates severely curved isopressure lines resulting from the rapid drop of the surface pressure after the ramp stop; the local pressure peak is located midway between the curved shock wave and the ramp surface. After the ramp motion ceases, the curved shock wave moves away from the surface and becomes straight in a considerable time. The surface pressure was found to reach its steady state value in about $30T$ (Fig. 1d).

Figure 4 contains the surface pressure variation during the compression-expansion-compression cycle of the moving ramp and isopressure contours at an instantaneous wedge angle when $\bar{\Omega}$ = 0.1. We note that the pressure change during the cycle shows severe hysteresis. We further note that the gap between the pressure during the upward motion and that during the downward motion is greater when the wedge angle is positive, which ,we consider, is due to the presence of the shock wave. The hysteretic behavior are better illustrated by pressure contours. The wedge angles at the instants marked by (1) and (2) are the same. The ramp

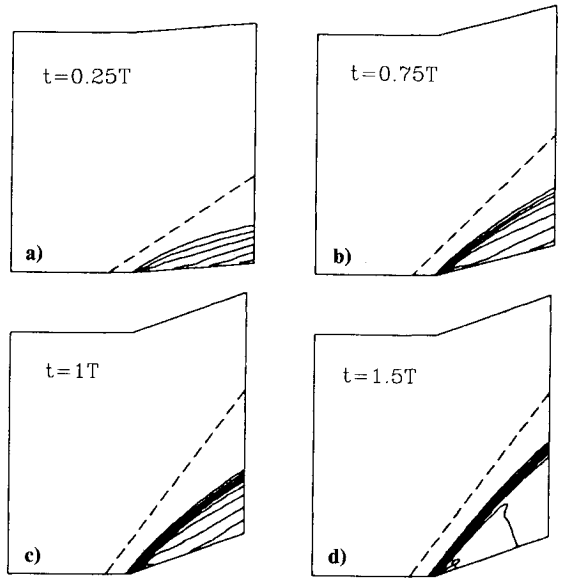

Fig. 2 Iso-pressure contours at various wedge angles, $\bar{\Omega}$ = 0.1.

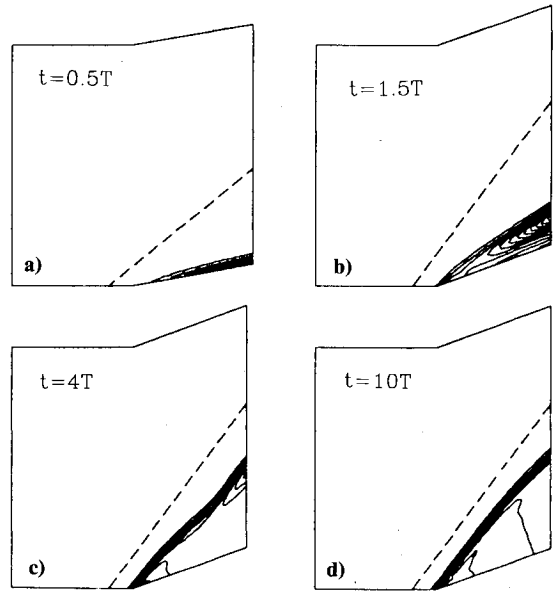

Fig. 3 Iso-pressure contours at various wedge angles, $\bar{\Omega}$ = 1.0.

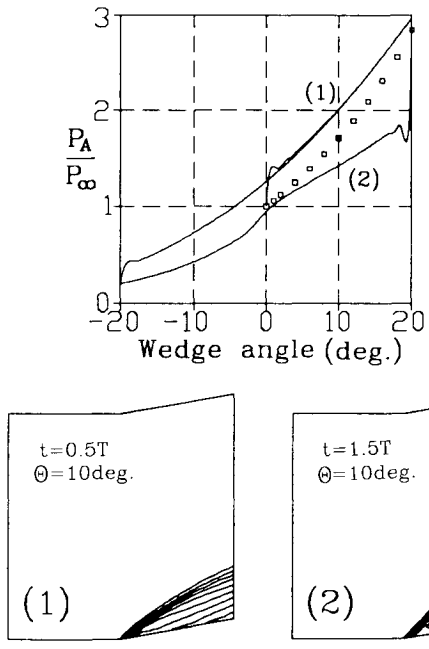

Fig. 4 Pressure variation and iso-pressure contours for the compression-expansion cycle ($\bar{\Omega}$ = 0.1).

at instant (1) is in upward motion, whereas at instant (2) it is in downward motion. As can be seen, the flow features at these times are quite different from each other. The surface pressure at instant (1) is much higher than that at instant (2) owing to the upward ramp motion (compressive stroke) though the shock wave is in formation stage. On the contrary, the shock wave at instant (2) is sharp. However, the surface pressure is much lower since the ramp moves downard (expansion stroke). When the ramp moved further downward so that the wedge angle became negative, an expansion fan was observed. When the ramp moved upward from −20 deg, we observed compression waves emanating from the surface and an expansion fan centered about the corner of the wedge.

Summary

Through numerical study using a moving grid system, inviscid supersonic flow past a moving compression ramp was investigated. The study revealed that the unsteady flow of the moving ramp could be considered steady or quasi-steady when $\bar{\Omega}$ was of order 0.01 or smaller. When $\bar{\Omega}$ was 0.1, the flow exhibited distinct unsteady behavior. The shock wave formed during the ramp motion was curved rather than straight. The surface pressure during the ramp motion was higher than the steady state value of the corresponding steady ramp. After the ramp motion ceased, it took a considerable time for the pressure to relax to the steady state value. When $\bar{\Omega} = 1.0$, the shock wave development was confined in the narrow region close to the moving surface. This shock wave then gradually moved away from the wall after the ramp stop and was finally developed to that of the steady state. When the ramp moved cyclically from −20 to 20 deg, hysteretic behavior of the flow was noticed.

References

[1]Degani, D., and Steger, J. L., "Comparison Between Navier-Stokes and Thin-Layer Computations for Separated Supersonic Flow," *AIAA Journal*, Vol. 21, No. 11, 1983, pp. 1604–1606.

[2]Hoffmann, K. A., *Computational Fluid Dynamics for Engineers, Engineering Education System*, Austin, TX, 1989, pp.402–403

[3]Kang, I. M. and Chang, K. S., "Euler Analysis of Transonic Stator-Rotor Interaction using a Finite Volume Method," *International Journal of Numerical Methods in Fluids*, Vol. 12, No. 7, 1991, pp. 625–636.

[4]Jameson, A., Schmidt, W., and Turkel, E., "Numerical Solutions of the Euler Equations by Finite Volume Methods using Runge-Kutta Time Stepping Schemes," AIAA Paper 81-1259, June 1981.

[5]Pulliam, T. H., "Artificial Dissipation Models for the Euler Equations," *AIAA Journal*, Vol. 24, No. 12, 1986, pp.1931–1940.

Concentration Measurements in a Transverse Jet by Planar Laser-Induced Fluorescence of Acetone

A. Lozano,* S. H. Smith,* M. G. Mungal,† and R. K. Hanson‡
Stanford University, Stanford, California 94305

I. Introduction

PLANAR laser-induced fluorescence (PLIF) is an attractive technique for concentration measurements in liquid and gaseous flows[1–3] because it is nonintrusive, effectively instantaneous, and provides concentration information in a whole plane without integration along the line of sight. Its use of molecular markers avoids problems of particle lag in fluid flow, and allows high spatial resolution measurements with minimal alteration of the flow conditions. However, although there is a large variety of potential tracers to be used in liquid flows, the selection is somewhat reduced when working with gases, and most chemicals currently used in gaseous PLIF concentration measurements (NO, I_2, biacetyl, or acetaldehyde) are not ideal for common experimental conditions, such as nonreacting turbulent flows at medium-high speeds and standard temperature and pressure. NO and I_2 have obvious toxicity, corrosion, and disposal problems. Acetaldehyde is carcinogenic, whereas biacetyl has a low vapor pressure and a peak absorption at a somewhat undesirable wavelength for current lasers, 420 nm. Recently, Lozano et al.[4] and Lozano[5] demonstrated the use of acetone as a concentration tracer in a small free air jet. Acetone was shown to be a convenient fluorescent marker when working in air flows, providing high signal-to-noise ratios (SNR). In the present work, acetone is used to obtain concentration images in a subsonic transverse air jet. Detection with a highly sensitive charged coupled device (CCD) camera has improved the data quality, decreasing the minimum detectable signal, increasing the SNR, and enabling the successful single-shot imaging of large fields of view (29×29 cm).

II. Tracer

Acetone is a very promising tracer for PLIF concentration measurements in gaseous flows, owing to its physical and photophysical characteristics. It has a high vapor pressure (~180 Torr at 20°C), which allows for high seeding densities, and its absorption band is broad (225–320 nm) with a maximum between 279 and 280 nm ($\sigma = 4.7 \times 10^{-20}$ cm^2). Acetone can, consequently, be excited using different commercially available lasers: a XeCl excimer (308 nm), a frequency-doubled dye laser operating with a red dye (e.g., Rhodamine 560, Rhodamine 590, or Kiton red), a fre-

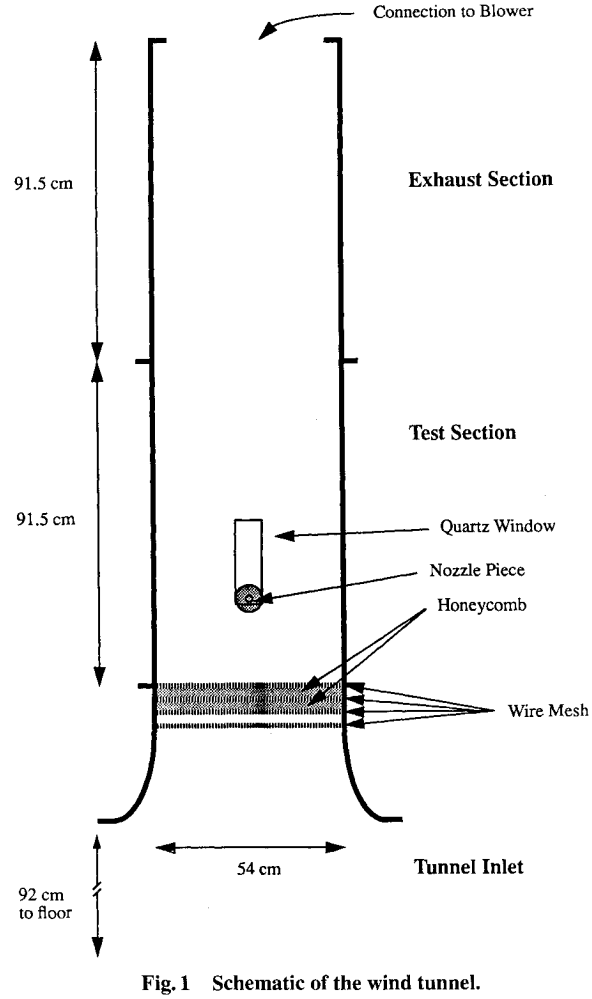

Fig. 1 Schematic of the wind tunnel.

Received Nov. 27, 1992; revision received May 25, 1993; accepted for publication May 26, 1993.

*Research Assistant, High Temperature Gasdynamics Laboratory, Department of Mechanical Engineering.

†Associate Professor, High Temperature Gasdynamics Laboratory, Department of Mechanical Engineering. Senior Member AIAA.

‡Professor, High Temperature Gasdynamics Laboratory, Department of Mechanical Engineering. Associate Fellow AIAA.